Rapid Communications

Angular momentum radiation from current-carrying molecular junctions

Zu-Quan Zhang [1,*] Jing-Tao Lü,[2,†] and Jian-Sheng Wang[1,‡]

[1]*Department of Physics, National University of Singapore, Singapore 117551, Republic of Singapore*

[2]*School of Physics and Wuhan National High Magnetic Field Center, Huazhong University of Science and Technology, 430074 Wuhan, People's Republic of China*

(Received 18 November 2019; revised manuscript received 13 March 2020; accepted 6 April 2020; published 22 April 2020)

We consider the radiation of angular momentum (AM) from current-carrying molecular junctions. Using the nonequilibrium Green's function method, we derive a convenient formula for the AM radiation and apply it to a prototypical benzene molecule junction. We discuss the selection rules for inelastic transitions between the molecular angular momentum eigenstates due to a sixfold rotational symmetry. Our study provides important insights into the generation of light with AM from DC-biased molecular junctions.

DOI: 10.1103/PhysRevB.101.161406

Introduction. The atomic scale interaction of nonequilibrium electrons with light is the key to develop electrically driven single molecular light sources for sensing, spectroscopy, and chemical reactions [1–3]. The high spatial resolution and local field enhancement offered by the tip of a scanning tunneling microscope provide an ideal platform to investigate this problem [4–9]. Recent years have witnessed tremendous progress in this direction. By analyzing the light emission spectra, a variety of physical and chemical information can be deduced, including vibrational coupling [7,10], coherent intermolecular dipole interaction [8,11,12], plasmon-exciton coupling [13,14], anti- and superbunching photon statistics [15,16], and charge and spin state emission [17,18]. A theoretical understanding of these effects relies on methods developed in quantum optics and quantum transport [18–27].

The coupling of electron orbital motion with its spin leads to spin-orbit interaction, which is of vital importance in spintronics [28], topological physics [29,30], and so on. Spin-orbit coupling is also responsible for the chiral-induced spin selectivity in electron transport through molecules [31,32]. However, the effect of electron orbital motion on single-molecule electroluminescence is, to a large extent, unexplored. In this work, based on the nonequilibrium Green's function (NEGF) method [33–36], we develop a microscopic theory to study electrically driven angular momentum emission from a single molecule. We consider a prototypical benzene molecule, which has well-defined orbital angular momentum states in an isolated situation. We illustrate the underlying mechanism as an inelastic electronic transition between states with different orbital angular momentum (AM). This is in contrast to the optical approach by passing normal light through constructed optical structures [37,38].

Theory. To consider an open system for light emission, we decompose it into four parts: a molecular system as a quantum emitter, the coupling of the quantum emitter with the radiation field, the radiation field itself, and the leads and their couplings with the quantum emitter for pumping energy and electrons into the quantum emitter.

We use a tight-binding (TB) model combined with the Peierls substitution [39] to describe the central molecule and its coupling with the radiation field, written as

$$H_t = \sum_{\langle ij\rangle} c_i^\dagger t_{ij} c_j e^{i\theta_{ij}}, \tag{1}$$

where $\langle ij\rangle$ denotes the nearest-neighbor (NN) sites i and j, t_{ij} is the NN hopping parameter, and $c_i^\dagger$ (c_i) is the electron creation (annihilation) operator at site i. The phase $\theta_{ij} = \frac{e}{\hbar}\int_{\boldsymbol{r}_j}^{\boldsymbol{r}_i} \boldsymbol{A}\cdot d\boldsymbol{l}$ represents the coupling to the radiation field. Here, $e \approx -1.602\times 10^{-19}$ C is the electron's charge, $\boldsymbol{A}$ is the vector potential, and $\boldsymbol{r}_i$ and $\boldsymbol{r}_j$ are the positions of sites i and j, respectively. Expanding $e^{i\theta_{ij}}$ in terms of $\boldsymbol{A}$ up to first order, we can write Eq. (1) into two terms $H_t \approx H_t^0 + H_{\rm int}$, with H_t^0 for the noninteracting electrons and $H_{\rm int}$ for the coupling of the electrons with the radiation field. They are given by

$$H_t^0 = \sum_{\langle ij\rangle} c_i^\dagger t_{ij} c_j, \tag{2}$$

$$H_{\rm int} \approx \sum_{\langle ij\rangle}\sum_{k}\sum_{\mu=x,y,z} M_{ij}^{k\mu} c_i^\dagger c_j A_\mu(\boldsymbol{r}_k), \tag{3}$$

where $M_{ij}^{k\mu} = i\frac{e}{2\hbar} t_{ij}(\boldsymbol{r}_i - \boldsymbol{r}_j)_\mu(\delta_{ki}+\delta_{kj})$ is the electron-photon coupling matrix element. We use Greek letters to represent components of the Cartesian coordinates, i.e., $\mu = x, y, z$.

The Hamiltonian of the radiation field is

$$H_{\rm rad} = \frac{1}{2}\int d^3\boldsymbol{r}\left(\varepsilon_0 \boldsymbol{E}_\perp^2 + \frac{1}{\mu_0}\boldsymbol{B}^2\right), \tag{4}$$

where ε_0 and μ_0 are the vacuum permittivity and permeability, respectively. Here, we adopt the Coulomb gauge with $\nabla\cdot\boldsymbol{A} =$

*phyzhaz@nus.edu.sg
†jtlu@hust.edu.cn
‡phywjs@nus.edu.sg

0, thus the transverse electric field is given by $\boldsymbol{E}_\perp = -\partial_t \boldsymbol{A}$, and the magnetic field is $\boldsymbol{B} = \nabla \times \boldsymbol{A}$. We restrict our discussion to the far-field radiation here and neglect the longitudinal electric field. The latter is important in the near-field region, such as near-field interactions and near-field heat transfer [40–42], while it decays with the distance much faster than the propagating transverse electromagnetic field and thus it is ignored in the far-field region. The effect of the leads and their couplings with the molecule are included by the self-energies, as shown below.

The energy and AM flux of electromagnetic field can be obtained from [43,44]

$$\boldsymbol{S} = \frac{1}{\mu_0}\langle : \boldsymbol{E}_\perp \times \boldsymbol{B} : \rangle, \tag{5}$$

$$\overleftrightarrow{\mathcal{M}} = \langle : \boldsymbol{r} \times \overleftrightarrow{\boldsymbol{T}} : \rangle, \tag{6}$$

where $\langle : AB : \rangle$ denotes normal order of operators AB when taking the ensemble average, which removes the zero-point motion contribution, and $\overleftrightarrow{\boldsymbol{T}}$ is the Maxwell stress tensor with $T_{\mu\nu} = \frac{1}{2}\delta_{\mu\nu}(\varepsilon_0 E^2 + \mu_0^{-1}B^2) - \varepsilon_0 E_\mu E_\nu - \mu_0^{-1} B_\mu B_\nu$. Equations (5) and (6) can be expressed in terms of the photon Green's function (GF) [45]

$$S^\mu(\boldsymbol{r}) = \epsilon_{\mu\nu\gamma}\epsilon_{\gamma\delta\xi}\frac{2}{\mu_0}\int_0^{+\infty}\frac{d\omega}{2\pi}\hbar\omega \times \mathrm{Re}\left[-\frac{\partial}{\partial x'_\delta}D^<_{\nu\xi}(\boldsymbol{r},\boldsymbol{r}',\omega)\right]\Big|_{\boldsymbol{r}'\to\boldsymbol{r}}. \tag{7}$$

The Einstein summation rule is used here, and $\epsilon_{\mu\nu\gamma}$ is the Levi-Civita symbol; $D^<_{\nu\xi}(\boldsymbol{r},\boldsymbol{r}',\omega)$ is the photon's lesser GF in the frequency domain. Relevant quantities in Eq. (6) are written as

$$\langle : E_\mu E_\nu : \rangle = \mathrm{Re}\left[\frac{2i}{\hbar}\int_0^\infty \frac{d\omega}{2\pi}(\hbar\omega)^2 D^<_{\mu\nu}(\boldsymbol{r},\boldsymbol{r},\omega)\right], \tag{8a}$$

$$\langle : B_\mu B_\nu : \rangle = \mathrm{Re}\left[i2\hbar\int_0^\infty \frac{d\omega}{2\pi}\epsilon_{\mu\gamma\xi}\epsilon_{\nu\gamma'\xi'} \times \frac{\partial}{\partial x_\gamma}\frac{\partial}{\partial x'_{\gamma'}}D^<_{\xi\xi'}(\boldsymbol{r},\boldsymbol{r}',\omega)\right]\Big|_{\boldsymbol{r}'\to\boldsymbol{r}}. \tag{8b}$$

The GFs are obtained following the standard NEGF formalism. The retarded GF is solved by the Dyson equation $D^r = d^r + d^r\Pi^r D^r$, and d^r is the free space photon GF [46]. The lesser GFs are obtained by the Keldysh equation $D^< = D^r\Pi^< D^a$, with $D^a = (D^r)^\dagger$. We use the random phase approximation to calculate the interacting self-energy

$$\Pi^<_{\mu\nu}(\boldsymbol{r}_i,\boldsymbol{r}_j,\omega) = -i\hbar\int_{-\infty}^{+\infty}\frac{dE}{2\pi\hbar}\mathrm{Tr}[M^{i\mu}g^<(E)M^{j\nu}g^>(E-\hbar\omega)], \tag{9}$$

where $\mathrm{Tr}[\cdots]$ means trace over the electron degrees of freedom, $g^{<(>)} = g^r\Sigma^{<(>)}_{\mathrm{leads}}g^a$ is the lesser (greater) GFs for the noninteracting electrons. Here, $\Sigma^{<(>)}_{\mathrm{leads}}$ is the lesser (greater) self-energy due to electron's coupling with the leads. The leads are in their respective equilibrium states and the self-energies follow the fluctuation-dissipation theorem, for lead β, $\Sigma^<_\beta = if_\beta\Gamma_\beta$ and $\Sigma^>_\beta = i(-1+f_\beta)\Gamma_\beta$. Here, $f_\beta(E,\mu_\beta) = 1/[\exp(\frac{E-\mu_\beta}{k_B T_\beta}) + 1]$ is the Fermi distribution function, μ_β is the chemical potential, T_β is the temperature, k_B is the Boltzmann constant, and $\Gamma_\beta = -2\mathrm{Im}[\Sigma^r_\beta]$ is the coupling-weighted spectrum of the lead.

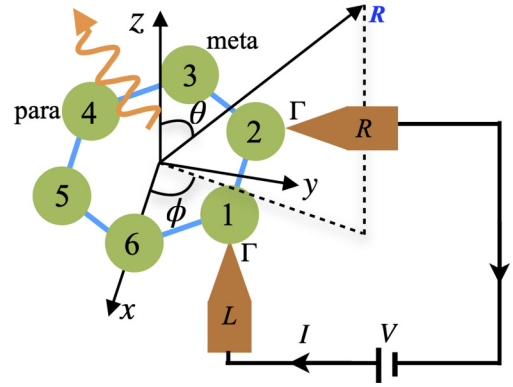

FIG. 1. Light emission from a benzene molecule junction. The metal leads L and R are connected to two carbon atoms in the *ortho* position. *Meta* and *para* positions correspond to lead R connecting to 3 and 4, respectively.

To calculate the total energy and AM radiation, we choose a large spherical surface enclosing the molecule, and perform the surface integral

$$P = \oint \boldsymbol{S}\cdot d\boldsymbol{A}, \tag{10}$$

$$\frac{d\boldsymbol{L}}{dt} = \oint \overleftrightarrow{\mathcal{M}}\cdot d\boldsymbol{A}, \tag{11}$$

where $d\boldsymbol{A} = \hat{\boldsymbol{R}}dA$, with $\hat{\boldsymbol{R}} = \boldsymbol{R}/R$ denoting the unit normal vector of the spherical surface dA with radius R. In the far-field region (with R much larger than the photon wavelength λ and the central molecule's size $\sim a$), we get simplified expressions for Eqs. (10) and (11) as

$$P = -\int_0^\infty \frac{d\omega}{2\pi}\frac{\hbar\omega^2}{3\pi\varepsilon_0 c^3}\mathrm{Im}\left[\Pi^{\mathrm{tot},<}_{\mu\mu}(\omega)\right], \tag{12}$$

$$\frac{dL_\gamma}{dt} = \int_0^\infty \frac{d\omega}{2\pi}\frac{\hbar\omega}{3\pi\varepsilon_0 c^3}\epsilon_{\gamma\mu\nu}\mathrm{Re}\left[\Pi^{\mathrm{tot},<}_{\mu\nu}(\omega)\right], \tag{13}$$

with $\Pi^{\mathrm{tot},<}_{\mu\nu}(\omega) = \sum_{ij}\Pi^<_{\mu\nu}(\boldsymbol{r}_i,\boldsymbol{r}_j,\omega)$. The Einstein summation rule is used here. We have performed the solid angle integration within the monopole approximation, i.e., neglecting the molecular size considering $(a/R) \ll 1$. We observe that the emission power is related to the trace, while the AM emission rate is related to the antisymmetric part of the tensor, $\Pi^{\mathrm{tot},<}$. Equation (13) is the main result of this Rapid Communication. It serves as a simple formula for calculating far-field radiation of optical AM from biased molecular systems. It can also be generalized to other interesting systems, such as two-dimensional sheets.

Application. The theory we develop is quite general. We now apply it to a prototypical benzene molecule junction shown in Fig. 1. We take the NN hopping parameter as $-t_{ij} = t = 2.5$ eV and the C-C bond length as $a = 1.4$ Å. We use the wideband approximation for molecule-lead coupling with $\Gamma_L = \Gamma_R = \Gamma$.

The isolated benzene molecule has a C_6 rotational symmetry. We put the molecule in the x-y plane with site

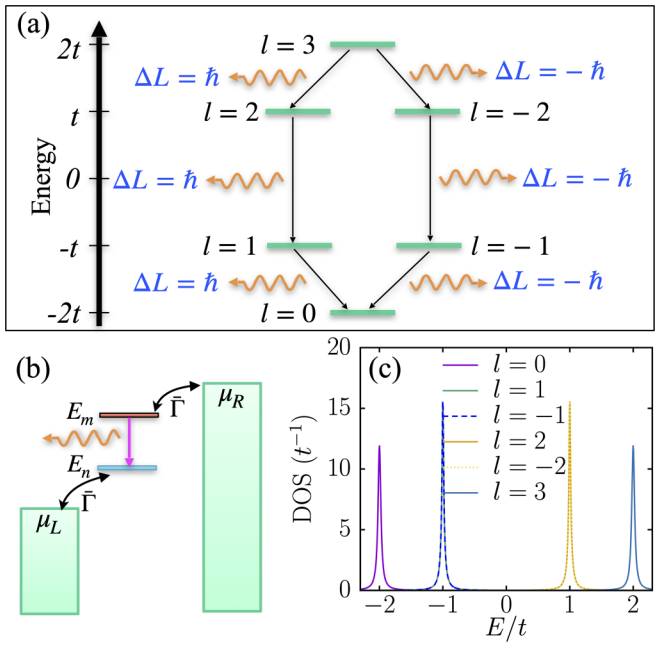

FIG. 2. (a) Selection rules for the emission of optical angular momentum between energy levels of the TB benzene molecule. (b) Light emission with leads coupled directly to two eigenmodes of the benzene molecule in high bias regime. $\bar{\Gamma}$ is the weak lead coupling to the modes. (c) Orbital resolved electron density of states (DOS) of the benzene molecule when coupled to the leads in the *ortho* position shown in Fig. 1, with $\Gamma = 0.4$ eV. The DOS is defined by $-\mathrm{Im}[\widetilde{g}^r_{ll}(E)]/\pi$ for energy level l.

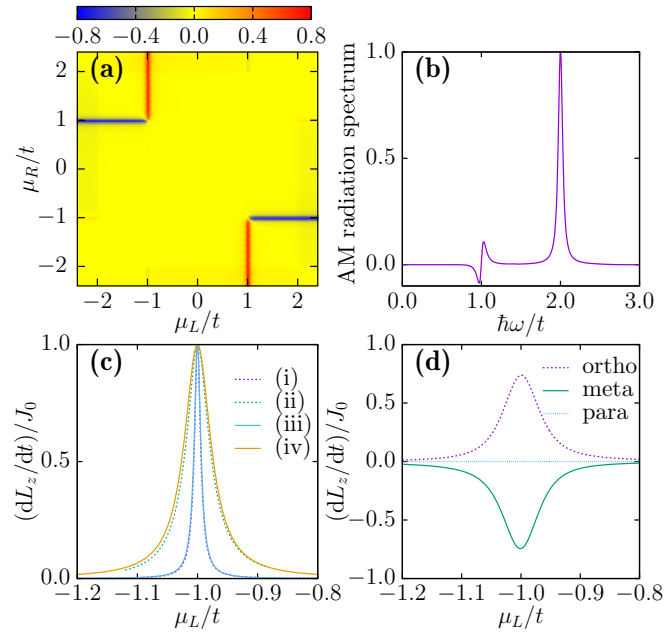

FIG. 3. (a) Intensity plot of angular momentum radiation rate normalized by $(dL_z/dt)/J_0$ as a function of chemical potentials μ_L/t and μ_R/t. (b) Frequency-resolved spectrum of the angular momentum radiation, normalized relative to the maximum value at $\hbar\omega = 2t$, for $\mu_L = -t$ and $\mu_R = 6$ eV. (c) Line cut of the plot in (a) at $\mu_R = 4$ eV. (i) and (ii) are results calculated from Eq. (13) at zero temperature, while (iii) and (iv) are results from Eq. (14). $\Gamma = 0.1$ eV for (i) and (iii), and $\Gamma = 0.4$ eV for (ii) and (iv). The leads couple to the benzene molecule in the *ortho* position for (a)–(c). For (c) and (d), $\mu_R = 4$ eV. For (a), (b), and (d), $\Gamma = 0.4$ eV, $T = 300$ K.

positions $x_j = a\cos(2\pi j/6)$, $y_j = a\sin(2\pi j/6)$, $j = 1, 2, \ldots, 6$. The orbital eigenenergies are $E_l = -2t\cos(2\pi l/6)$, with $l = 0, \pm1, \pm2, 3$. We have neglected the spin degeneracy here. When coupled to the two metal leads, the energy levels are broadened, but the degeneracy is not lifted. The orbital resolved density of states (DOS) is shown in Fig. 2(c). Here the mode space GF $\widetilde{g}^r$ is related to the real space GF via the unitary transformation $\widetilde{g}^r = U^\dagger g^r U$, with $U_{jm} = e^{i2\pi jm/6}/\sqrt{6}$, $j, m = 1, 2, \ldots, 6$. Note that the mode index m is unique only modulo 6, thus 6 is the same as 0, and 5 is the same as -1. Also, we use the notation that an operator denoted as O in real space is written as $\widetilde{O}$ in mode space, with $\widetilde{O} = U^\dagger O U$.

The mechanism of AM emission can be understood by considering the selection rules in mode space. Defining the electron velocity matrix $v^\mu_{ij} = t_{ij}(\boldsymbol{r}_i - \boldsymbol{r}_j)_\mu/\hbar$, we have $v^\mu = \frac{1}{ie}\sum_k M^{k\mu}$, which has the C_6 rotational symmetry. For the coordinate system we choose here, the C_6 symmetry leads to the relations $\widetilde{v}^x_{nm}\widetilde{v}^x_{mn} = \widetilde{v}^y_{nm}\widetilde{v}^y_{mn}$ and $\widetilde{v}^x_{nm}\widetilde{v}^y_{mn} = i\Delta_{mn}\widetilde{v}^x_{nm}\widetilde{v}^x_{mn}$. Here, $\Delta_{mn} = \mathrm{sgn}(m-n)$ if $|m-n| = 1$, and $\Delta_{16} = -\Delta_{61} = 1$, otherwise $\Delta_{mn} = 0$.

We consider the simple case where the leads couple respectively to only two eigenmodes of the molecule in the high bias regime $\mu_L \ll E_n < E_m \ll \mu_R$ [Fig. 2(b)]. In the limit $\bar{\Gamma} \to 0$, we get from Eq. (12) $P = -\omega^2_{mn}e^2(\widetilde{v}^x_{nm}\widetilde{v}^x_{mn} + \widetilde{v}^y_{nm}\widetilde{v}^y_{mn})/(3\pi\varepsilon_0 c^3)$, and $dL_z/dt = i\omega_{mn}e^2(\widetilde{v}^x_{nm}\widetilde{v}^y_{mn} - \widetilde{v}^y_{nm}\widetilde{v}^x_{mn})/(3\pi\varepsilon_0 c^3)$ from Eq. (13), with $\hbar\omega_{mn} = E_m - E_n$ [45]. Using the relations of the velocity matrix due to the C_6 symmetry, we get $\frac{dL_z/dt}{P} = \frac{\Delta_{mn}}{\omega_{mn}}$. This result is reminiscent of Eq. (19) of a recent work for the classical case of AM radiation from a single electron performing circular motion with a constant frequency [47]. Since every emitted photon carries an energy $\hbar\omega_{mn}$, the number of photons emitted per unit time is $dN/dt = P/(\hbar\omega_{mn})$. Thus, the AM per emitted photon is $\Delta L = \frac{dL_z/dt}{dN/dt} = \Delta_{mn}\hbar$, which is the selection rules shown in Fig. 2(a).

The light emission for real-space coupling in Fig. 1 is a combination of all the possible processes shown in Fig. 2(a). This is tuned by the applied bias. Significant light emission between two energy levels of the molecule is possible when the energy levels enter into the bias window, restricted by the selection rules. Since the degenerate energy levels ($l = \pm1, \pm2$) are broadened but not split when the molecule couples to the leads, they will enter into or out of the bias window simultaneously. Light emission from inelastic transition $l = 2 \to l = 1$ is accompanied by emission from transition $l = -2 \to l = -1$. These two processes emit light with opposite AM. The summation of the two leads to cancellation of the total AM.

Figure 3(a) shows the intensity plot of total AM radiation as a function of the two chemical potentials μ_L and μ_R in the *ortho* position. We observe a four-line-segment feature (FLSF) where the AM radiation is large when one chemical potential is in resonance with the eigenstates at $\pm t$ and the bias

window covers the energy range $[-t, t]$. The AM radiation is quite small in other regions. To analyze this resonant effect, we show in Fig. 3(b) the frequency/energy-resolved spectrum of the AM radiation [Eq. (13) without frequency integration] for the resonant case. There is a large peak at $\hbar\omega = 2t$, which implies that the FLSF in Fig. 3(a) is contributed mainly from the radiative transition processes $l = 2 \to l = 1$ and $l = -2 \to l = -1$.

Why does it generate net AM radiation? It seems not so obvious considering that photons emitted by the two transitions are opposite polarized and the degeneracy of the involved orbital states is not lifted due to lead couplings [see Fig. 2(c)]. To analyze this, we performed a simplified analysis using only these four modes, $l = \pm 1, \pm 2$. We find that the cross correlations between the degenerate states, such as $\tilde{g}^r_{15}(E)$ and $\tilde{g}^r_{24}(E)$, are more important in the generation of net AM radiation than the correlations between nondegenerate states, such as $\tilde{g}^r_{12}(E)$ and $\tilde{g}^r_{14}(E)$. We set the latter to 0 for simplicity. With these simplifications, for the resonant peak at $\mu_L = -t$, we get from Eq. (13) in the zero-temperature limit [45]

$$\frac{dL_z}{dt} \approx J_0 \frac{(\Gamma/6)^2}{(\mu_L + t)^2 + (\Gamma/6)^2}, \tag{14}$$

with $J_0 = \frac{2}{\sqrt{3}\pi} t\alpha(v_0/c)^2$, $v_0 = at/\hbar$, the fine-structure constant $\alpha = e^2/(4\pi\varepsilon_0\hbar c)$, and the light speed c. The approximate expression of Eq. (14) agrees well with numerical results from Eq. (13) [Fig. 3(c)]. Equation (14) implies that the height of the resonance peak is a constant at zero temperature, and its width is characterized by $\Gamma/6$.

Figure 3(d) shows the AM radiation for different ways of connecting the leads. For the *ortho* position, the resonant peak is broadened and its height is reduced, compared to the zero-temperature result (ii) in Fig. 3(c). This is due to a higher temperature at 300 K. For the asymmetric couplings at the *meta* position, the AM radiation shows resonant effect, similar to the result at the *ortho* position but with the opposite direction of AM. However, for the symmetric couplings at the *para* position, the net AM is 0 despite the applied biases. These properties imply the possibility to design smart optical devices that can control the generation of AM radiation by simply applying an electric bias to the molecule junction, a convenient way compared with controlling AM radiation using a temperature bias [48,49] or an external magnetic field [50].

In the analysis of the experimental optical spectra of the benzene molecule, electronic transitions with vibronic couplings are considered. Though only the electronic excitations are considered in our model, the main features of the AM radiation corresponding to the electronic transitions $l = \pm 2 \to l = \pm 1$ with a transition energy of $2t = 5.0$ eV, may be observed qualitatively in the future experiment, referring to the typical lowest electronic transition ${}^1B_{2u} \leftarrow {}^1A_{1g}$ with an absorption peak at $E \approx 4.9$ eV in experiments [51,52].

Conclusion. In summary, using the NEGF method, we have developed a theoretical framework to study AM radiation from current-carrying molecular junctions. As an application, the theory identifies from a quantum viewpoint that electrons of a ringlike benzene molecule emit light with AM due to radiative transitions between different angular momentum states. Due to asymmetric couplings to the leads and electron tunneling between degenerate energy states with opposite angular momentum, large resonant effect with the bias potential was discovered. Our theory can be straightforwardly applied to more realistic chiral molecules. One possible application of our study is that single molecular junction is promising in optical antennas [26] to control emission polarization and directivity by lead touching and the applied electrical bias.

Acknowledgments. Z.-Q.Z. and J.-S.W. acknowledge the support by MOE tier 2 Grant No. R-144-000-411-112 and FRC Grant No. R-144-000-402-114. J.-T.L. is supported by the National Natural Science Foundation of China under Grant No. 21873033.

[1] M. Galperin and A. Nitzan, Phys. Chem. Chem. Phys. **14**, 9421 (2012).
[2] S. V. Aradhya and L. Venkataraman, Nat. Nanotechnol. **8**, 399 (2013).
[3] K. Kuhnke, C. Große, P. Merino, and K. Kern, Chem. Rev. **117**, 5174 (2017).
[4] R. Berndt, J. K. Gimzewski, and P. Johansson, Phys. Rev. Lett. **67**, 3796 (1991).
[5] R. Berndt, R. Gaisch, J. K. Gimzewski, B. Reihl, R. R. Schlittler, W. D. Schneider, and M. Tschudy, Science **262**, 1425 (1993).
[6] J. Aizpurua, G. Hoffmann, S. P. Apell, and R. Berndt, Phys. Rev. Lett. **89**, 156803 (2002).
[7] X. H. Qiu, G. V. Nazin, and W. Ho, Science **299**, 542 (2003).
[8] Z.-C. Dong, X.-L. Guo, A. S. Trifonov, P. S. Dorozhkin, K. Miki, K. Kimura, S. Yokoyama, and S. Mashiko, Phys. Rev. Lett. **92**, 086801 (2004).
[9] N. L. Schneider, G. Schull, and R. Berndt, Phys. Rev. Lett. **105**, 026601 (2010).
[10] C. Chen, P. Chu, C. A. Bobisch, D. L. Mills, and W. Ho, Phys. Rev. Lett. **105**, 217402 (2010).
[11] Y. Zhang, Y. Luo, Y. Zhang, Y.-J. Yu, Y.-M. Kuang, L. Zhang, Q.-S. Meng, Y. Luo, J.-L. Yang, Z.-C. Dong, and J. G. Hou, Nature (London) **531**, 623 (2016).
[12] H. Imada, K. Miwa, M. Imai-Imada, S. Kawahara, K. Kimura, and Y. Kim, Nature (London) **538**, 364 (2016).
[13] Y. Zhang, Q.-S. Meng, L. Zhang, Y. Luo, Y.-J. Yu, B. Yang, Y. Zhang, R. Esteban, J. Aizpurua, Y. Luo, J.-L. Yang, Z.-C. Dong, and J. G. Hou, Nat. Commun. **8**, 15225 (2017).
[14] H. Imada, K. Miwa, M. Imai-Imada, S. Kawahara, K. Kimura, and Y. Kim, Phys. Rev. Lett. **119**, 013901 (2017).
[15] L. Zhang, Y.-J. Yu, L.-G. Chen, Y. Luo, B. Yang, F.-F. Kong, G. Chen, Y. Zhang, Q. Zhang, Y. Luo, J.-L. Yang, Z.-C. Dong, and J. G. Hou, Nat. Commun. **8**, 580 (2017).
[16] C. C. Leon, A. Rosławska, A. Grewal, O. Gunnarsson, K. Kuhnke, and K. Kern, Sci. Adv. **5**, eaav4986 (2019).
[17] B. Doppagne, M. C. Chong, H. Bulou, A. Boeglin, F. Scheurer, and G. Schull, Science **361**, 251 (2018).

[18] K. Miwa, H. Imada, M. Imai-Imada, K. Kimura, M. Galperin, and Y. Kim, Nano Lett. **19**, 2803 (2019).

[19] M. Galperin and A. Nitzan, Phys. Rev. Lett. **95**, 206802 (2005).

[20] N. L. Schneider, J. T. Lü, M. Brandbyge, and R. Berndt, Phys. Rev. Lett. **109**, 186601 (2012).

[21] J.-T. Lü, R. B. Christensen, and M. Brandbyge, Phys. Rev. B **88**, 045413 (2013).

[22] F. Xu, C. Holmqvist, and W. Belzig, Phys. Rev. Lett. **113**, 066801 (2014).

[23] K. Kaasbjerg and A. Nitzan, Phys. Rev. Lett. **114**, 126803 (2015).

[24] L.-L. Nian, Y. Wang, and J.-T. Lü, Nano Lett. **18**, 6826 (2018).

[25] J. Kröger, B. Doppagne, F. Scheurer, and G. Schull, Nano Lett. **18**, 3407 (2018).

[26] M. Parzefall and L. Novotny, Rep. Prog. Phys. **82**, 112401 (2019).

[27] S. Mukamel and M. Galperin, J. Phys. Chem. C **123**, 29015 (2019).

[28] D. Awschalom and N. Samarth, Physics **2**, 50 (2009).

[29] M. Z. Hasan and C. L. Kane, Rev. Mod. Phys. **82**, 3045 (2010).

[30] X.-L. Qi and S.-C. Zhang, Rev. Mod. Phys. **83**, 1057 (2011).

[31] K. Ray, S. P. Ananthavel, D. H. Waldeck, and R. Naaman, Science **283**, 814 (1999).

[32] S. Dalum and P. Hedegård, Nano Lett. **19**, 5253 (2019).

[33] H. Haug and A.-P. Jauho, *Quantum Kinetics in Transport and Optics of Semiconductors* (Springer, Berlin, 1996).

[34] H. Bruus and K. Flensberg, *Many-Body Quantum Theory in Condensed Matter Physics: An Introduction* (Oxford University Press, New York, 2004).

[35] J.-S. Wang, J. Wang, and J. T. Lü, Eur. Phys. J. B **62**, 381 (2008).

[36] J.-S. Wang, B. K. Agarwalla, H. Li, and J. Thingna, Front. Phys. **9**, 673 (2014).

[37] S. Zhang, H. Wei, K. Bao, U. Håkanson, N. J. Halas, P. Nordlander, and H. Xu, Phys. Rev. Lett. **107**, 096801 (2011).

[38] Y. Gorodetski, A. Drezet, C. Genet, and T. W. Ebbesen, Phys. Rev. Lett. **110**, 203906 (2013).

[39] M. Graf and P. Vogl, Phys. Rev. B **51**, 4940 (1995).

[40] A. I. Volokitin and B. N. J. Persson, Rev. Mod. Phys. **79**, 1291 (2007).

[41] Z.-Q. Zhang, J.-T. Lü, and J.-S. Wang, Phys. Rev. B **97**, 195450 (2018).

[42] J.-S. Wang, Z.-Q. Zhang, and J.-T. Lü, Phys. Rev. E **98**, 012118 (2018).

[43] S. M. Barnett, J. Opt. B **4**, S7 (2002).

[44] M. Janowicz, D. Reddig, and M. Holthaus, Phys. Rev. A **68**, 043823 (2003).

[45] See Supplemental Material at http://link.aps.org/supplemental/10.1103/PhysRevB.101.161406 for details on the derivation of the radiation formulas, the derivation of the selection rules for the tight-binding benzene molecule, the analysis of the resonant effect, and the radiation patterns of energy and angular momentum. The Supplemental Material includes Refs. [23,44,46,47].

[46] O. Keller, *Quantum Theory of Near-Field Electrodynamics* (Springer, Berlin, Germany, 2012).

[47] M. Katoh, M. Fujimoto, H. Kawaguchi, K. Tsuchiya, K. Ohmi, T. Kaneyasu, Y. Taira, M. Hosaka, A. Mochihashi, and Y. Takashima, Phys. Rev. Lett. **118**, 094801 (2017).

[48] M. F. Maghrebi, A. V. Gorshkov, and J. D. Sau, Phys. Rev. Lett. **123**, 055901 (2019).

[49] C. Khandekar and Z. Jacob, Phys. Rev. Appl. **12**, 014053 (2019).

[50] A. Ott, P. Ben-Abdallah, and S.-A. Biehs, Phys. Rev. B **97**, 205414 (2018).

[51] E. Pantos, J. Philis, and A. Bolovinos, J. Mol. Spectrosc. **72**, 36 (1978).

[52] I. Borges, A. Varandas, A. Rocha, and C. Bielschowsky, J. Mol. Struct., THEOCHEM **621**, 99 (2003).